

Hydrodynamic and geometric effects in the sedimentation of model run-and-tumble bacteria

A. Scagliarini^{1,2,*} and I. Pagonabarraga^{3,4,5}

¹*IAC-CNR, Istituto per le Applicazioni del Calcolo “Mauro Picone”, Via dei Taurini 19, 00185 Rome, Italy.*

²*INFN, sezione Roma “Tor Vergata”, via della Ricerca Scientifica 1, 00133 Rome, Italy*

³*CECAM, Centre Européen de Calcul Atomique et Moléculaire,*

Ecole Polytechnique Fédérale de Lausanne, Batochimie, Avenue Forel 2, 1015 Lausanne, Switzerland

⁴*Departament de Física de la Matèria Condensada,*

Universitat de Barcelona, Martí i Franquès 1, 08028 Barcelona, Spain

⁵*Universitat de Barcelona, Institute of Complex Systems (UBICS),*

Universitat de Barcelona, 08028 Barcelona, Spain

The sedimentation process in a suspension of bacteria is the result of the competition between gravity and the intrinsic motion of the microorganisms. We perform simulations of run-and-tumble “squirmers” that move in a fluid medium, focusing on the dependence of the non-equilibrium steady state on the bacterial swimming properties. We find that for high enough activity, the density profiles are no longer simple exponentials; we recover the numerical results via the introduction of a local effective temperature, suggesting that the breakdown of the Perrin-like exponential form is a collective effect due to the onset of fluid-mediated dynamic correlations among particles. We show that analogous concepts can fit also the case of shakers, for which we report the first study of this kind. Moreover we provide evidences of scenarios where the solvent hydrodynamics induces non-local effects which require the fully three-dimensional dynamics to be taken into account in order to understand sedimentation of active suspensions. Finally, analyzing the statistics of the bacterial swimming orientations, we discuss the emergence of polar order in the steady state sedimentation profiles.

I. INTRODUCTION

A number of microorganisms (bacteria, algae, etc...) have the ability to swim in a liquid environment through the generation of autonomous motion at expenses of their metabolism, thus being intrinsically out-of-equilibrium. As such, these systems lead to new challenges such as the understanding of how collective phenomena and self-organization emerge from the relevant features of their propulsion mechanism [1–4]. In this perspective a suspension of active particles is qualitatively different from a suspension of passive ones. Maybe the simplest, yet not trivial, example of this is the case of a constant external forcing on the suspension, such as gravity in the sedimentation process. In fact, when thermal fluctuations are negligible (as it is in the case of particles above the micron size), while passive particles would inevitably precipitate, active suspensions maintain a finite sedimentation length that grows with the self-propulsion speed. This result was predicted theoretically for “dry” suspensions (i.e. where the solvent hydrodynamics is neglected) of non-interacting run-and-tumble particles [5, 6] and, then, confirmed in numerical simulations with point-like dipoles [7] and experimentally in suspensions of active colloids [8]. Suspensions of self-propelled particles under gravity have been also reported to display a non-trivial orientational dynamics, with the development of an associated polar order [9, 10] or even, in the case of

bottom-heavy particles, to the inversion of the sedimentation profiles [11]. In this paper we present a computational study of bacterial sedimentation, where hydrodynamics is fully resolved near and far from the swimmer’s surface. We provide evidence that hydrodynamic correlations induce important deviations from the phenomenology for dry suspensions in the steady state of both self-propelled swimmers and “shakers” (for which, to the best of our knowledge, this represents the first study of this kind). The sedimentation profiles observed when bacterial activity is intense are captured through a simple extension of a drift-diffusion model with height dependent effective temperature. We show that pullers develop a distal region of constant density (a supernatant) whose emergence depends on both the activity/gravity ratio and on the confining geometry (i.e. the cell aspect-ratio). We also address the statistics of the orientation of bacterial swimming, finding that, in the regime of small tumbling frequency, the suspension develops a polar order whose characteristics are strongly dependent on the type of swimmer.

II. NUMERICAL METHOD AND SIMULATION DETAILS

The velocity field of the solvent (of dynamic viscosity η) is evolved by means of a lattice Boltzmann (LB) method [12] with nineteen lattice speeds in three dimensions (D3Q19) [13]. Swimmers are modelled as solid spherical objects of radius R . The correct momentum exchange and mass conservation through the set of bound-

* andrea.scagliarini@cnr.it

any links (between grid points in and out the sphere) representing the particles is implemented according to the bounce-back-on-links scheme [14–16]. In order to mimic the surface deformations inducing microswimmers’ self-propulsion, we adopt a simplified version [17] of the “squirmer” model [18, 19], whereby only the first two terms in the series expansion of the axisymmetric surface slip velocity profile are retained, thus leaving just two relevant parameters, dubbed B_1 and B_2 . The first is related to the propulsion speed, which is $\mathbf{v}_p = \frac{2}{3}B_1\hat{m}$, where \hat{m} is the squirmer orientation unit vector, defining the instantaneous swimming direction. The second parameter, B_2 , determines the strength of the stresslet, $\mathcal{S} \propto \eta R^2 B_2$, generated by the swimmer in the surrounding fluid (and, hence, it is related to the amplitude of the injected vorticity) [19]. The ratio $\beta \equiv \frac{B_2}{B_1}$, such that $\beta \in (-\infty, +\infty)$, quantifies the relative intensity of apolar stresses and polar self-propulsion and classifies swimmers in “pushers”, $B_2 < 0$ (including bacteria like, e.g. *E. Coli*), “pullers”, $B_2 > 0$ (as the alga *Chlamydomonas*), and “potential” swimmers, $\beta = 0$ (i.e. swimmers that simply self-propel without generating vorticity, like the alga *Volvox carteri* or certain artificial swimmers) [19–23]. Every τ time steps the particles randomize their orientation \hat{m} , thus accounting for the characteristic “run-and-tumble” mechanism, which can be seen as a source of diffusion for particles that, we recall here, are insensitive to thermal fluctuations. It is worth noticing that our model, featuring finite size resolved particles, equipped with the squirming motion, is able to capture hydrodynamic effects in the sedimentation of active suspensions, both in their near and far field manifestations.

We simulate suspensions, of volume fraction $\phi = 0.07$, in three-dimensional boxes of size $L \times L \times H$, with height $H \approx 80R$ and variable aspect-ratio $\Gamma = L/H$. Two solid walls (with no-slip boundary condition for the fluid velocity) confine the system in the z -direction, while periodic boundary conditions along x, y apply. The number of particles, with radius $R = 2.3$ (in lattice-spacing units), range between ~ 500 and $\sim 3 \times 10^4$. We introduce a reference velocity, $v_g = \mu F_g / (6\pi\eta R)$ (where F_g is the gravity force magnitude and $\mu = 1/(6\pi\eta R)$ is the particle mobility), i.e. the sedimentation velocity of a passive particle, and a reference time, $t_c = R/v_p$, that is basically the time an isolated particle takes to displace its own radius. In terms of v_g and t_c , the following dimensionless parameters can be defined, namely:

$$\chi_1 = \frac{v_p}{v_g} = \frac{2B_1}{3v_g}; \quad \chi_2 = \frac{v_{B_2}}{v_g} = \frac{B_2}{3v_g}; \quad \bar{\tau} = \frac{\tau}{t_c}, \quad (1)$$

that, together with β , govern the squirmers motion. In order to investigate how the bacterial swimming characteristics and the system geometry affect the sedimentation profiles, we performed several runs exploring the parameter space spanned by $(\chi_1, \chi_2, \beta, \Gamma)$ (the tumbling rate will be fixed to $\bar{\tau} \approx 4.3$, unless differently specified).

III. BACTERIAL DENSITY PROFILES

We start each run with the bacteria homogeneously distributed in space, with random orientations. To check that a (non-equilibrium) statistically steady state is reached, we follow the time evolution of the average height $h(t) = \frac{1}{H} \int_0^H z \rho(z, t) dz$, where $\rho(z, t)$ is the (unsteady) normalized particle density (i.e. $\rho(z, t) dz$ is the probability of finding a bacterium centred between z and $z + dz$ at the time t). We consider as steady state the time interval during which $h(t)$ fluctuates by less than $\sim 5\%$. All data shown hereafter are meant averaged over such time interval. Our aim is to study the impact that activity, in terms of χ_1 and β , has on the squirmer sedimentation, and to characterize the emerging dynamical regimes, checking whether and how hydrodynamic effects come into play. According to the theory [5, 6], as $\chi_1 \rightarrow 1$, all particles concentrate at the bottom wall. Instead, when $\chi_1 \gg 1$ (i.e., in the self-propulsion dominated regime) the steady state sedimentation profile should display an exponential form $\rho(z) \sim e^{-z/\lambda}$, with a sedimentation length depending on the single particle velocity (and, hence, on χ_1) as

$$\lambda = \frac{v_p^2 \tau}{3v_g} = \frac{\ell}{3} \chi_1, \quad (2)$$

where $\ell = v_p \tau$ is the bacterium run length. This result has been found in agreement with experimental observations [8] and numerical simulations [7]. The exponential profile characterizes also equilibrium systems, as in the classical Perrin’s experiment for (thermal) colloids [24]; the sedimentation length is determined by the particle diffusivity, D , and the gravity force as $\lambda^{(eq)} = D/(\mu F_g)$ and depends, therefore, through the Stokes-Einstein relation $D = \mu k_B T$, on the system temperature T , namely $\lambda^{(eq)} = k_B T / F_g$. The formal analogy with the passive (equilibrium) case suggests, then, to introduce an *effective* temperature as:

$$k_B T_{\text{eff}}^{(1p)} = \frac{v_p^2 \tau}{3\mu}, \quad (3)$$

such that the sedimentation length reads $\lambda = k_B T_{\text{eff}}^{(1p)} / F_g$. In Fig. 1 we plot the time-averaged steady state bacterial density profiles for various values of χ_1 and $\beta = 0$. For values close to one, as expected, bacteria uniformly fall down under the action of gravity; however, due to the particles finite size, the sedimentation length remains finite. The particles in the sediment tend to organize themselves in layers with crystal-like order, noticeable from the peaks in the density profile, close to the bottom wall, displaced from each other by about one diameter ($2R$), as found also in a previous computational study [10]. At increasing χ_1 , swimmers occupy an increasingly larger volume of liquid, and correspondingly $\rho(z)$ shows, over the whole box length, the predicted exponential profile [6], with a sedimentation length growing

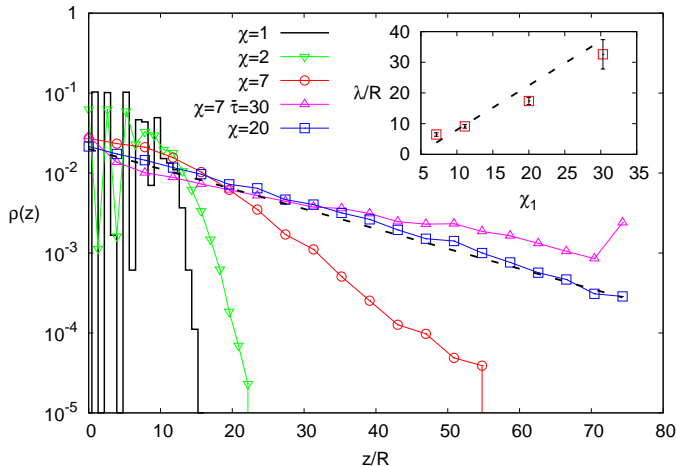


FIG. 1. MAIN PANEL: Density profiles $\rho(z)$ for various values of the gravity/propulsion ratio χ_1 , at $\beta = 0$. For χ_1 close to one, bacteria accumulate at the bottom wall, showing crystal order (as the regularly spaced peaks in ρ suggest). For large χ_1 the expected exponential profile is recovered. INSET: Dependence of the sedimentation length λ (computed out of exponential fits of the bacterial density profiles) (\square) on the propulsion/gravity ratio χ_1 . The dashed line depicts the theoretical expectation $\lambda/\chi_1 = \ell/3 \approx 1.45R$, Eq. (2), valid for $\chi_1 \gg 1$.

linearly with χ_1 (see inset of Fig. 1).

If we increase $|\beta|$ (thus intensifying bacterial activity) to large enough values, for a fixed χ_1 , the deviation from the exponential profile can be important, as one can see from Fig. 2, where we plot the bacterial density $\rho(z)$ for three cases with same $\chi_1 = 10$ but with different β . In the pushers/pullers case ($\beta \neq 0$), dynamic correlations are so intense that recovering a Perrin-like form just with the introduction of a global effective diffusion coefficient as coming from *single* particle is no longer possible [8]. The larger $|\beta|$, the stronger is the departure of the sedimentation profile from an exponential; indeed we found that deviations start to be relevant from $|\beta| \approx 5$ on. This observation may justify why in a previous numerical study of sedimenting bacteria with hydrodynamic interactions [7] (whose force dipole model would give an equivalent $\beta = -1$) apparently no significant effects were detected.

IV. EXTENDED DIFFUSIVE MODEL

Due to hydrodynamic correlations the dynamics of a bacterium in the suspension is affected by the presence of the others through the generation of motion within the liquid, which will act as a “bath” at an effective temperature (that measures the fluid “agitation”). We can understand these effects extending a diffusive model proposed earlier to describe bacterial sedimentation [8], based on

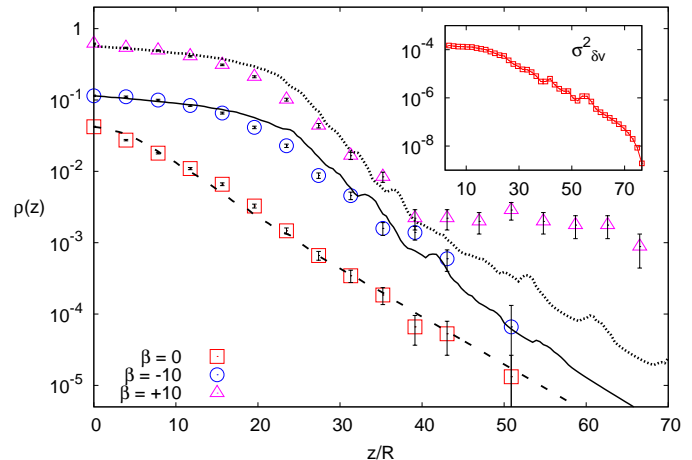


FIG. 2. MAIN PANEL: Density profiles for squirmers with $\chi_1 = 10$ and $\beta = 0, \pm 10$ (data are vertically shifted for clarity). The lines represent the predictions coming from the numerical integration of Eq. (6) with $\lambda = 15$ and $\alpha_1 = 1$ (see the text for the discussion of the model parameters) for $\beta = 0$ (dashed line), $\beta = -10$ (solid line) and $\beta = +10$ (dotted line). INSET: Fluid velocity fluctuations $\sigma_{\delta u}^2(z) = \sum_{i=1}^3 \langle (u_i(\mathbf{r}, t) - \langle u_i(\mathbf{r}, t) \rangle)^2 \rangle$ as a function of the system height for the case $\beta = -10$.

the Smoluchowski equation $\partial_t \rho = -\nabla \cdot \mathbf{J}$, determined by the flux $\mathbf{J} = -\tilde{D} \nabla \rho + \tilde{\mu} \mathbf{F}_g \rho$. The ratio of the *local* diffusion coefficient, \tilde{D} , and particle mobility, $\tilde{\mu}$, by virtue of a generalized Stokes-Einstein relation, represents the effective temperature field. Assuming that in the steady state the density will only depend on z (we will come back later to the validity of this assumption), the zero flux boundary conditions at the walls gives:

$$\frac{d\rho}{dz} = -\frac{F_g}{k_B T_{\text{eff}}} \rho. \quad (4)$$

We propose an effective temperature of the form $T_{\text{eff}} = T_{\text{eff}}^{(1p)} + T_{\text{eff}}^{(\text{coll})}$, consisting of two terms: the single-particle effective temperature, Eq. (3), accounting for the self-propulsion, plus a contribution proportional to fluid velocity fluctuations, $T_{\text{eff}}^{(\text{coll})}$, capturing the collective effects due to hydrodynamic interactions. However, since in the steady state bacteria are distributed inhomogeneously over the volume (with a density increasing from top to bottom), also fluid velocity fluctuations $\sigma_{\delta u}^2 = \sum_{i=1}^3 \langle (u_i(\mathbf{r}, t) - \langle u_i(\mathbf{r}, t) \rangle)^2 \rangle$ (where $\langle (\dots) \rangle = \frac{1}{L^2} \int \int (\dots) dx dy$) are expected to vary (as indeed it can be seen in the inset of Fig. 2). We should then cope with a height dependent effective temperature $T_{\text{eff}}(z) = T_{\text{eff}}^{(1p)} + T_{\text{eff}}^{(\text{coll})}(z)$, leading, upon insertion in (4), to an equation for the sedimentation density which can be re-

cast in the following form

$$\frac{d\rho}{dz} = -\frac{1}{\lambda} \frac{\rho}{\left(1 + \frac{T_{\text{eff}}^{(\text{coll})}(z)}{T_{\text{eff}}^{(1p)}}\right)}, \quad (5)$$

where $\lambda = (k_B T_{\text{eff}}^{(1p)})/F_g$ is the sedimentation length discussed in the previous section. We assume, then, $T_{\text{eff}}^{(\text{coll})}(z) \propto \sigma_{\delta u}^2(z)$ to hold, so that we can finally write

$$\frac{d\rho}{dz} = -\frac{1}{\lambda} \frac{\rho}{\left(1 + \alpha_1 \frac{\sigma_{\delta u}^2(z)}{v_p^2}\right)}, \quad (6)$$

with α_1 a free parameter representing the proportionality constant between $T_{\text{eff}}^{(\text{coll})}$ and $\sigma_{\delta u}^2$. Comparing the numerical integration of Eq. (6) with data from LB simulations (see Fig. 2), we find that the proposal of gauging the global effective temperature to a height dependence works well for $\beta = 0$ and $\beta < 0$. The phenomenology of pullers ($\beta > 10$) appears, however, to be more complicated: in fact, while the density profile can be recovered where the concentration is higher, the presence of a region of constant density, denoting the formation of a supernatant floating over the sedimentated layer, eludes the generalized diffusive model.

V. THE CASE OF “SHAKERS”

Another striking instance of how crucial the role played by hydrodynamics can be is provided by the regime where $|\beta| \rightarrow \infty$, i.e. B_1 goes to zero while B_2 stays finite. This regime corresponds to active suspensions where particles do not self-propell but generate motion in the fluid and are relevant for microswimmers known as “shakers” [1, 25], like, e.g., melanocytes [26]. Since both their propelling velocity and the effect of thermal fluctuations are negligible, such a suspension would undergo a gravitational collapse, if one could completely neglect the presence of the solvent. However, as shown in Fig. 3, the steady state density profiles develop a sedimentation layer, whose width increases with χ_2 . The observed width cannot be interpreted simply as a result of the close-packing of the particles, which would imply, in fact, a value of around $8R$, much smaller than the measured one. We try to recover the sedimentation profiles of shakers following the same ideas of the previous section. We must integrate numerically an analogue of Eq. (6), the main difference being that now the one-particle contribution to the effective temperature $T_{\text{eff}}^{(1p)}$ is zero, since an isolated shaker does not self-propell, so that we get $T_{\text{eff}}(z) = T_{\text{eff}}^{(\text{coll})}(z) = \alpha_2(\sigma_{\delta u}^2(z)/v_{B_2}^2)$ (here we indicate the phenomenological parameter as α_2 in order to distinguish it from that of propellers). The reference speed $v_{B_2} = B_2/3$, implicitly introduced in (1), is the magnitude of the velocity field generated by an isolated shaker, averaged over its surface. The stationary Smoluchowski

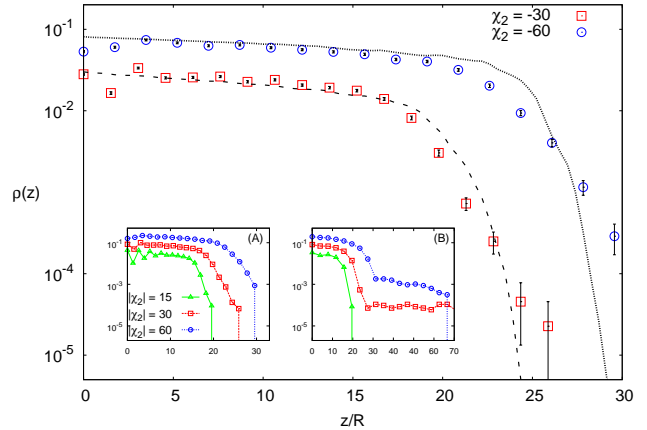


FIG. 3. MAIN PANEL: Density profiles for shakers with two different $\chi_2 < 0$ (here and in the insets data are vertically shifted for clarity): the larger $|\chi_2|$ the longer the density tail (i.e. the wider is the region occupied by particles). The lines are the theoretical predictions coming from the numerical integration of Eq. (7), where the function $\sigma_{\delta u}^2(z)$ is taken from the simulations, with $\alpha_2 = 4.4$. INSET A: Density profiles for shakers with negative χ_2 . INSET B: Density profiles for shakers with positive χ_2 : notice the formation of the supernatant for large enough χ_2 .

equation, then, reads:

$$\frac{d\rho}{dz} = -\frac{F_g}{\alpha_2} \frac{\rho}{(\sigma_{\delta u}^2(z)/v_{B_2}^2)}; \quad (7)$$

the results of the numerical integration of Eq. (7) for shakers with negative χ_2 with two different values of gravity are reported in Fig. 3, showing, again, good agreement. Analogously to the case of pullers, shakers with $\chi_2 > 0$ develop (for χ_2 large enough) a distal region of constant density in the sedimentation profile (see inset B of Fig. 3). The emergence of such supernatant is due to the sedimentate which acts as a pump and generates motion in higher layers of fluid. It is, then, a genuinely *three-dimensional* and *non-local* effect, two features which make also our formalism based on a height dependent effective temperature fail. To support this picture, we show that, for a fixed value of χ_2 the supernatant disappears when decreasing the aspect-ratio Γ of the cell below unity (see Fig. 4). This is, indeed, a manifestation of three-dimensionality: using an analogy with a Rayleigh-Bénard system [27], we argue that the geometry favors (or not) the development of a large scale flow which can (or can not) sustain the supernatant. In fact, the difference in the fluid flow pattern generated by a single particle, either a pusher or a puller, is not strong enough to sustain the different macroscopic patterns observed if the swimmers are randomly oriented (as a matter of fact, no supernatant is observed for pushers, or shakers, with $\beta < 0$). Hence, a collective organization of the swimmers is required to produce the observed macroscopic flows.

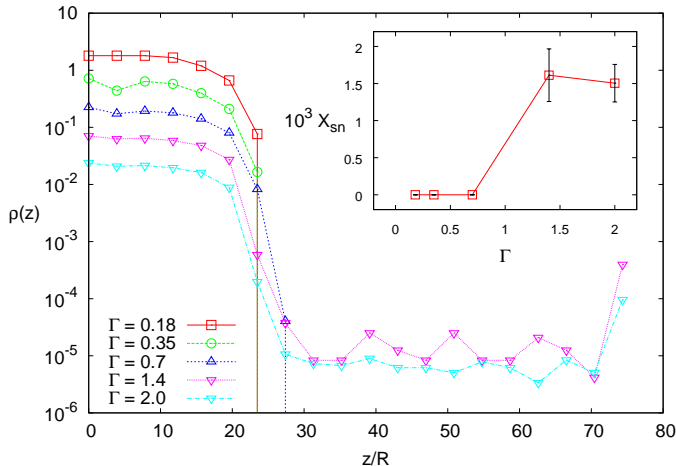


FIG. 4. MAIN PANEL: Density profiles for shakers with $\chi_2 = 8.3$ for various aspect-ratios $\Gamma = L/H$ (data are vertically shifted for clarity). INSET: Fraction of particles in the supernatant region, computed as $X_{sn} = \int_{\zeta_0}^H \rho(z) dz$ (ζ_0 being the minimum height such that $\rho(z) = 0$, for some Γ and for $z > \zeta_0$), as function of the aspect-ratio of the cell: notice that for $\Gamma < 1$, $X_{sn} = 0$, i.e. no supernatant develops.

We will next address the emergence of orientational order in the sedimenting profiles of microswimmers.

VI. ORIENTATIONAL STATISTICS

The emergence and the dynamical relevance of anisotropic ordering in active fluid systems has been widely recognized in the literature [1, 9, 28]. We study the orientational statistics measuring the PDF $\rho(z^*, e_z)$ of the z -component of the bacterial *squirring* characteristic vector, e_z , within slabs of width $4R$ centred at different heights z^* along the cell. For squirmers with $\chi_1 = 10$, $\beta = 0$ and tumbling time $\bar{\tau} \approx 4.3$ we find a bimodal distribution symmetrically peaked at $e_z = \pm 1$ (with a slight imbalance towards $e_z = -1$) and almost insensitive to changes in z^* . However, for $\bar{\tau} \approx 30$, we observe that, close to the wall, the peak in $\rho(z^* = 2R, -1)$ is more pronounced than that in $\rho(z^* = 2R, +1)$, whereas the opposite trend appears at $z^* = 18R$ (see Fig. 5), which means that in the bulk bacteria swim preferentially upwards (i.e. against gravity). Previous theoretical studies have predicted the emergence of polar order when bacterial self-propulsion dominates over thermal noise [9]. In our athermal case, where tumbling plays the role of an effective noise, the higher the tumbling rate (short $\bar{\tau}$) the closer is the dynamics to thermal diffusion. Therefore, we need to increase $\bar{\tau}$ in order to favour the *active* diffusion due to self-propulsion and, consequently, the suspension polarization. Analogously, for $\beta \neq 0$ we expect this scenario to break down, because the generation of fluid motion acts as an effective source of “noise”; indeed, we

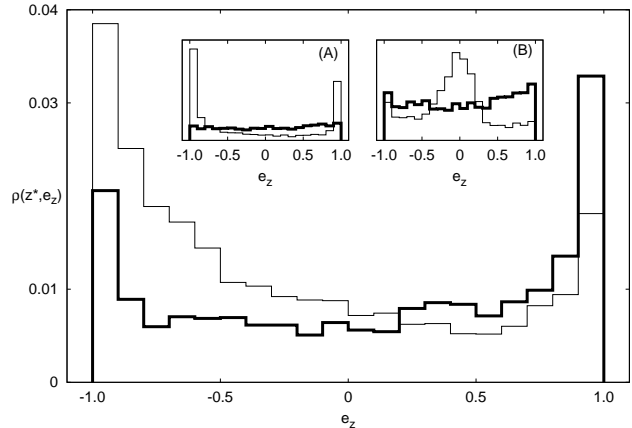


FIG. 5. Probability distributions of the vertical component of bacterial orientation, e_z , measured inside two slabs $[z^* - 2R, z^* + 2R]$, with $z^* = 2R$ (thin line) and $z^* = 18R$ (thick line), respectively. MAIN PANEL: Potential swimmers ($\beta = 0$). INSET A: Pullers ($\beta > 0$). INSET B: Pushers ($\beta < 0$). In all cases $\chi_1 = 10$ and $\bar{\tau} \approx 30$.

observe that, close to the wall, $\rho(z^*, e_z)$ is peaked around $e_z \approx 0$ for $\beta < 0$, and it is bimodal (with a higher at $e_z \approx -1$) for $\beta > 0$, while in the bulk it is rather uniform in both cases (insets A and B of Fig. 5). As anticipated in the previous section, such different orientational ordering between pushers and pullers turns out to have an impact also on the swimmers’ distribution in space, as indicated by the sedimentation profiles.

VII. CONCLUSIONS

We have presented a computational study of suspensions of run-and-tumble squirmers under gravity. Thanks to the built-in properties of the mesoscopic approach adopted we could take into account both the finite size of particles and the hydrodynamics of the solvent. In the case of potential swimmers, agreement has been found with theoretical predictions regarding i) the dependence of the density profiles on the activity/gravity ratio and ii) the emergence of a polar order from the inspection of distributions of particle orientations. We have reported evidence that, for pushers and pullers with large enough β , the hydrodynamic flows induced by their collective motion determine sedimentation profiles that cannot be understood in terms of single swimmer response to the gravitational field. This observation appeared particularly distinctive in the emblematic case of shakers. We have, therefore, generalized the theory on the basis of a height dependent *collective* effective temperature. Moreover, we have provided instances of cases (i.e. pullers and shakers with positive β) where, due to the fluid flow and to a non-trivial organization of swimmers, the full *three-dimensional* dynamics must be considered for the sake of

a satisfactory understanding of the sedimentation phenomenology.

ACKNOWLEDGEMENTS

We acknowledge MICINN and DURSI for financial support under Projects No. PGC2018-098373-B-I00, and

No. 2017SGR- 884, respectively. IP acknowledges SNSF for financial support under Project No. 200021-175719. This work was possible thanks to the access to MareNostrum Supercomputer at Barcelona Supercomputing Center (BSC) and also through the Partnership for Advanced Computing in Europe (PRACE).

-
- [1] M. Marchetti, J.-F. Joanny, S. Ramaswamy, T. Liverpool, J. Prost, M. Rao, and R. Simha, *Rev. Mod. Phys.* **85**, 1143 (2013).
 - [2] J. Elgeti, R. Winkler, and G. Gompper, *Rev. Prog. Phys.* **78**, 056601 (2015).
 - [3] R. Simha and S. Ramaswamy, *Phys. Rev. Lett.* **89**, 058101 (2002).
 - [4] I. Llopis and I. Pagonabarraga, *Europhys. Lett.* **75**, 999 (2006).
 - [5] J. Tailleur and M. Cates, *Phys. Rev. Lett.* **100**, 21803 (2008).
 - [6] J. Tailleur and M. Cates, *Europhys. Lett.* **86**, 60002 (2009).
 - [7] R. Nash, R. Adhikari, J. Tailleur, and M. Cates, *Phys. Rev. Lett.* **104**, 258101 (2010).
 - [8] J. Palacci, C. Cottin-Bizonne, C. Ybert, and L. Bocquet, *Phys. Rev. Lett.* **105** (2010).
 - [9] M. Enculescu and H. Stark, *Phys. Rev. Lett.* **107**, 058301 (2011).
 - [10] J.-T. Kuhr, J. Blaschke, F. Rühle, and H. Stark, *Soft Matter* **13**, 7548 (2017).
 - [11] K. Wolff, A. Hahn, and H. Stark, *Eur. Phys. J. E* **36**, 43 (2013).
 - [12] S. Succi, *The lattice Boltzmann equation for complex states of flowing matter* (Oxford University Press, 2018).
 - [13] J.-C. Desplat, I. Pagonabarraga, and P. Bladon, *Comp. Phys. Comm.* **134**, 273 (2001).
 - [14] A. Ladd, *J. Fluid Mech.* **271**, 285 (1994).
 - [15] A. Ladd, *J. Fluid Mech.* **271**, 311 (1994).
 - [16] N.-Q. Nguyen and A. Ladd, *Phys. Rev. E* **66** (2002).
 - [17] R. M. Navarro and I. Pagonabarraga, *Eur. Phys. J. E* **33**, 27 (2010).
 - [18] J. Blake, *J. Fluid Mech.* **46**, 199 (1971).
 - [19] T. Ishikawa, M. Simmonds, and T. Pedley, *J. Fluid Mech.* **568**, 119 (2006).
 - [20] M. Lighthill, *Comm. Pure Appl. Math.* **5**, 109 (1952).
 - [21] K. Drescher, R. Goldstein, N. Michel, M. Polin, and I. Tuval, *Phys. Rev. Lett.* **105**, 168101 (2010).
 - [22] S. Thutupalli, R. Seemann, and S. Herminghaus, *New J. Phys.* **13**, 073021 (2011).
 - [23] A. Evans, T. Ishikawa, T. Yamaguchi, and E. Lauga, *Phys. Fluids* **23**, 111702 (2011).
 - [24] J. Perrin, *Ann. Chim. Phys.* **8**, 5 (1909).
 - [25] S. Ramachandran, P. S. Kumar, and I. Pagonabarraga, *Eur. Phys. J. E* **20**, 151 (2006).
 - [26] H. Gruler, U. Dewald, and M. Eberhardt, *Eur. Phys. J. B* **11**, 187 (1999).
 - [27] S. Chandrasekhar, *Hydrodynamic and hydromagnetic stability* (Oxford University Press, 1961).
 - [28] S. Ramaswamy, *Annu. Rev. Cond. Matter Phys* **1**, 323 (2010).